



## The Geometry of Coronary Artery Bifurcations and Its Role in Plaque Formation

Alberto Otero-Cacho<sup>1,2</sup> and Alberto P Muñozuri<sup>1\*</sup>

### Affiliation

<sup>1</sup>Department of Physics, Universidade de Santiago de Compostela, Spain

<sup>2</sup>Flow Reserve Labs SL Edificio Emprendia, Spain

\* **Corresponding author:** Department of Physics, Universidade de Santiago de Compostela, Spain, Email: [alberto.perez.munuzuri@usc.es](mailto:alberto.perez.munuzuri@usc.es)

**Citation:** Otero-Cacho A and Muñozuri AP. The geometry of coronary artery bifurcations and its role in plaque formation (2022) Clinical Cardiol Cardiovascular Med 4: 24-30.

**Received:** Dec 11, 2021

**Accepted:** Feb 12, 2022

**Published:** Feb 18, 2022

**Copyright:** © 2022 Otero-Cacho A, et al., This is an open-access article distributed under the terms of the Creative Commons Attribution License, which permits unrestricted use, distribution, and reproduction in any medium, provided the original author and source are credited.

### Abstract

The risk of cardiovascular diseases is determined by the deposition of plaque in the coronary arteries. The areas of plaque deposition are also controlled by the flow dynamics and, for this, the topology of the arterial bifurcations has shown to be crucial. We present a detailed analysis of different topologies at the bifurcation based on numerical simulations of a mathematical model. Different diameters of the involved vessels as well as angle between them are analyzed. Unexpectedly, the curvature of the walls connecting the vessels is observed to play an important role.

**Keywords:** Atherosclerosis, Blood flow, Bifurcation.

**Abbreviation:** WSS-Wall Shear Stress, FVM-Finite Volume Method, Re-Reynolds Number,  $R_v$ -Radius of Curvature.

### Introduction

According to World Health Organization data, cardiovascular diseases represent the most frequent cause of death worldwide. Among these diseases, atherosclerosis which develops unevenly along the coronary tree, remains the leading cause of death. Influence of vessel geometry and hemodynamic characteristics on the development of vascular pathologies as atherosclerosis was demonstrated through several studies and Wall Shear Stress (WSS) has been shown to play a key role in the evolution of blood vessel diameter due to the accumulation of plaque. Among other locations, several studies have indicated that arteries that bifurcate are more prone to develop atherosclerotic lesions. The morphology of the coronary bifurcations varies depending on their location in the coronary artery tree. In addition, a specific bifurcation may change its morphology due to an intervention, for example, after the placement of a stent. On other hand, it is widely known that areas with low WSS are more prone to plaque formation. There are several ways to measure WSS and criteria to characterize those areas that could potentially be more affected by atherosclerosis. One of these methods is to find the minimum value of the wall shear stress. Another way to identify these areas of larger probability of developing atherosclerosis is by setting a WSS value below which we consider that the deposition of plaque is more likely to occur [1-12].

This value is quite variable. While some studies consider that this value should be set to 0.4 Pa [4], others consider that deposition takes place when the value of WSS does not exceed 1 Pa [13] or 1.26 Pa [14]. Morbiducci, et al., (2016) [15] review the factors affecting WSS and plaque formation, reaching the conclusion that geometry together with other biological and hemodynamic factors decisively affect plaque

formation. Pinho, et al., (2019) [16] and Gallo, et al., (2012) [17] use in their studies real artery geometries extracted from a medical image. Whereas Pinho, et al., (2019) [16] observe that lower values of parameters such as tortuosity or cross-sectional area of the right ventricular branch lead to hemodynamic conditions susceptible to atheroma formation, Gallo, et al., (2012) [17] demonstrate that there is a strong relationship between helical flow patterns and exposure to disturbed shear on carotid bifurcation. Other factors such as the presence of stenosis [18,19], angle of bifurcation [11,19,20] and the elastic behavior of the walls [21] have an influence on the evolution of the plaque formation and the distribution of pressure in the blood vessels.

A recent result by Otero-Cacho, et al., (2018) [11] demonstrated the important role played by the bifurcations in the coronary tree and their geometry in plaque deposition. Compared to the existing literature, our work focuses on the topology of the vertex itself whose anatomical differences are as numerous as vessels. Their effect on the plaque formation risk will be analyzed for a wide range of different idealized configurations. Furthermore, other parameters such as the opening angle and the blood vessel diameter are studied together to better understand their influence in the flow distribution. The morphological differences of the bifurcations that are found in the human body are very diverse. Nevertheless, analyzing some simplified geometries enlightens the type of problems and phenomena that can be observed in real more-complex geometries. Of all bifurcations in the coronary system, LM-LAD-LCx bifurcations are most often affected by disease [15].

Thus, along this manuscript we will consider different idealized symmetric and non-symmetric geometries describing an idealized vessel bifurcation based on LM-LAD-LCx bifurcations and other common configurations in the coronary system. Also, the geometrical specificities of the bifurcation itself will be considered in detail as they play an important role in the local flow. The paper is organized as follows. After the introduction, the details of the simulated model are presented as well as the numerical methods to solve it. The results section is divided into two subsections. The first part is devoted to understanding the role played in the blood circulation by the actual geometry of the bifurcation vertex itself. This case is analyzed, for simplicity, considering a symmetrical bifurcation. The second part of the results deals with non-symmetric bifurcations and the effect of the bifurcation angle and the vessels diameters in order to identify those areas more prone to plaque formation. The final section presents the conclusions of the study.

## Material and Methods

### Geometries

**Symmetric bifurcations:** The first part of the results is dedicated to the influence of the topology of the bifurcation itself on the WSS distribution and, consequently, on the possible plaque deposition. For this study and for simplicity, we consider a symmetric bifurcation so that the effect of the vertex geometry is not masked by other factors. Thus, all the vessels considered are endowed with the same diameter. Thus, a mother vessel of 2mm of diameter splits in two daughter vessels each with the same diameter ( $D_1 = D_2 = D_3 = 2$  mm). To characterize the topology of the bifurcation, two parameters are introduced in the model that describe, on the one hand, the transition from the mother vessel wall into the outer walls of the two daughter vessels. This is described by the radius of curvature of the outer wall at the bifurcation ( $R_o$ ). On the other hand, we also considered the curvature of the wall that provides the transition between the two daughter vessels. And this value is measured by the radius of curvature  $R_v$ . **Figure 1** presents a scheme of the symmetric configuration with the control parameters ( $R_o$  and  $R_v$ ) marked on it.

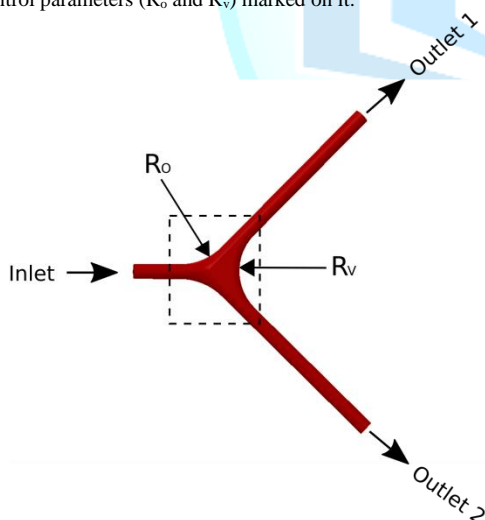


**Figure 1:** General scheme of a symmetric bifurcation. Minimum values of wall shear stress are located right after the main vessel splits in two daughter vessels.  $R_o$  is the curvature radius of outer wall.  $R_v$  is the curvature radius of vertex or the wall connecting both daughter vessels.

**Non-symmetric bifurcations:** Two idealized different configurations of non-symmetric bifurcations are studied. In the first configuration, the proximal main vessel diameter ( $D_1$ ) is kept equal to the distal main vessel diameter  $D_3$  ( $D_1 = D_3 = 2$ mm). The side branch diameter ( $D_2$ ) varies from 0.5 to 2 mm. On the other hand, and for the other

configuration mentioned before, we consider an approximation to the observed situation in coronary arteries that the vessels tend to decrease their diameter after a bifurcation. This decrease in the diameters has been modelled by the Finet's Law [22] that is widely used in clinical applications [23,24] and it is expressed by,

$$D_1 = 0.678 \cdot (D_2 + D_3) \quad (1)$$

Thus, for the second non-symmetric configuration used we strictly apply the Finet's law. The inlet diameter of the proximal main vessel is always kept equal to  $D_1 = 2$ mm for all the simulations. Three different diameters (1.0, 1.5 and 2.0 mm) are considered for the side branch and the distal main vessel diameters are calculated using the formula above. In order to keep consistency with experimental evidence, the distal main vessel diameter is always considered smaller than the diameter of the proximal main vessel [25]. Four different bifurcation angles are considered ( $20^\circ$ ,  $40^\circ$ ,  $60^\circ$ ,  $90^\circ$ ) for both configurations. A general scheme with the main control parameters for our simulations as well as the notation used is presented in **Figure 2**.

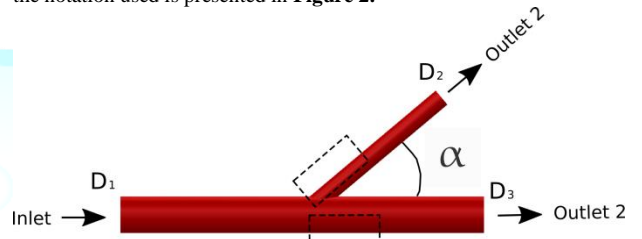


**Figure 2:** General scheme for the non-symmetric bifurcation.

Minimum values of wall shear stress are typically located in the outer wall of the side branch and the main vessel right after the bifurcation (areas marked with a dashed box in the figure). The control parameters in the simulations are the angle ( $\alpha$ ) and the different diameters of the vessels involved.

**Mesh:** A 3D mesh is built using Simcenter Star-CCM+ software [26]. In general, cells of arbitrary polyhedral shape are used in most of the volume. The mesh is refined in the vicinity of the walls using hexahedral layers in order to detect more precisely the behavior of the fluid in these areas. To ensure that the results do not depend on the mesh used, three grids of different grid density and size are considered, and all the simulations were run using all the meshes considered (**Figure 3**).

Maximum velocity and minimum WSS values are the target observables studied for each mesh. The difference among them is less than 5% in every configuration. Details of the grid analysis for an angle  $\alpha=20^\circ$  and a non-symmetric bifurcation with the first configuration ( $D_1 = D_3$ ) are presented in **Table 1**.

### Mathematical model and simulation settings

The mathematical model considered for our results discretizes the incompressible Navier-Stokes equations using the Finite-Volume Method (FVM). The flow field is governed by the continuity and momentum Navier-Stokes equations [27].

$$\nabla \cdot \vec{v} = 0 \quad (2)$$

$$\rho(\vec{v} \cdot \nabla) \vec{v} = -\nabla p + \mu \nabla^2 \vec{v} \quad (3)$$

Where  $\vec{v}$  is the flow velocity,  $\rho$  is the density,  $\mu$  is the dynamic viscosity and  $p$  is the pressure.

Simcenter Star-CCM+ software is used to design the geometries, build the mesh and carry out numerical simulations. Segregated flow solver (SIMPLE algorithm) [28] was used to solve the integral conservation equations of mass and momentum in a sequential manner. This solver employs a pressure-velocity coupling algorithm where the mass conservation constraint on the velocity field is fulfilled by solving a pressure-correction equation [26].

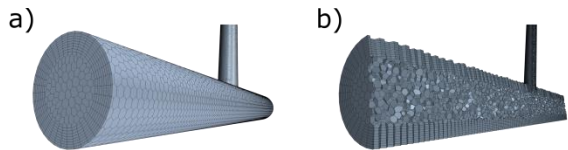


**Figure 3:** a) Surface mesh in a  $\alpha=60^\circ$  geometry. b) Detail of the mesh inside the geometry. Polyhedral elements form the central part of the geometry whereas a refinement is applied near the wall.

	No. of cells	Parameters		Variations	
		Max. Velocity (m/s)	Min. WSS (Pa)	Max. Velocity	Min. WSS (Pa)
Grid 1	91255	0.364398	0.60718	-	-
Grid 2	72893	0.364298	0.613959	0.03%	1.10%
Grid 3	63378	0.366394	0.612039	0.69%	0.79%

Note: Non-symmetric bifurcation ( $D_1=D_2=2\text{mm}$ ;  $D_3=1\text{mm}$ ,  $\alpha=20^\circ$ )

**Table 1:** Grid analysis. Velocity and WSS values for different grids for the non-symmetric case ( $D_1=D_3=2\text{mm}$ ;  $D_2=1\text{mm}$ ,  $\alpha=20^\circ$ ). Equivalent analysis was performed for all the other configurations considered with similar results (not presented here).

Circulating blood flow is modeled as an incompressible Newtonian fluid whose density is kept constant and equal to  $1060 \text{ kg/m}^3$  and viscosity  $0.004 \text{ Pa}\cdot\text{s}$  [11,29]. Vessel walls are assumed to be rigid boundaries with no-slip condition, constant velocity of  $0.2 \text{ m/s}$  is set at the inlet [30] and atmospheric pressure at the outlets [31,32]. A specific case with different boundary conditions has been studied for the case of symmetric bifurcations and its description is found in the Supplementary Information. Reynolds numbers smaller than 400 are always considered for all the configurations (thus laminar flow is always granted). The mesh considered is formed by polyhedral and rectangular prisms arranged in the following way: polyhedral prisms occupy the central part of the geometry whereas rectangular prisms are used to create thin layers of elements that help us to accurately capture the phenomena that occur near the wall (see Figure 3 for details). The convergence criterion of reduction of residuals by five orders of magnitude is used and computations are run until a steady state is reached.

## Results

### Effect of the vertex topology

Previous reports analyzing the effect of bifurcations on the circulating flow usually considered an idealized bifurcation characterized by a sharp vertex. The actual geometry of the bifurcation in real situations is far more complicated and, in this section, we analyze the effect of its main topological features on blood circulation. Under experimental conditions, the transition from the proximal main vessel to the distal main vessel and branch vessel is smooth and may present a large variety of configurations. In order to incorporate the most of them, two parameters are introduced in the vertex geometry that try to emulate conditions closer to experiments. The two parameters (introduced in Figure 1) describe the radius of curvature of the outer wall at the bifurcation ( $R_o$ ) and the radius of curvature of the inner wall at the bifurcation ( $R_v$ ). In all simulations the inner diameters of all the vessels are kept constant and equal ( $D_1 = D_2 = D_3$ ) and the bifurcation, for simplicity, is considered symmetric (as in Figure 1). In the analysis of the simulations below and as mentioned in the introduction, we focus on the Wall Shear Stress (WSS) as it has been shown to be a good marker of regions with high potentiality to present pathological plaque deposition [9,10].

In Figure 4, a summary of the different configurations is presented. Figs. 4a to 4c show different configurations varying the inner vertex curvature ( $R_v$ ). The values of the WSS are color coded in the same figures. It is clearly observed that increasing  $R_v$  results in a larger area

of low values of WSS and larger vascular risk. The areas where WSS is lower than  $1 \text{ Pa}$  are measured for each experiment and the values are plotted versus  $R_v$  in Figure 4d. This curve clearly shows the important role played by the inner radius of curvature on the extension of the risky areas. The effect of the outer radius of curvature,  $R_o$ , is shown in Figures. 4e to 4h. Figure 4e to 4g present different geometries of the bifurcation for the different values of  $R_o$  considered. Here, also the areas of low WSS (lower than  $1 \text{ Pa}$ ) are color coded. All the values of the areas of low WSS are plotted versus  $R_o$  in Figure 4h.

Note that the effect of the outer radius of curvature is much less significant than  $R_v$ , although it is still possible to observe some slight increase in the areas with  $R_o$  and, thus, some increase in the coronary risk. Equivalent simulations are done considering a pulsatile flow and outlet pressure conditions and the results agree with those presented above. The inlet velocity profile is extracted from bibliography [30] and it is described in Figure 5.

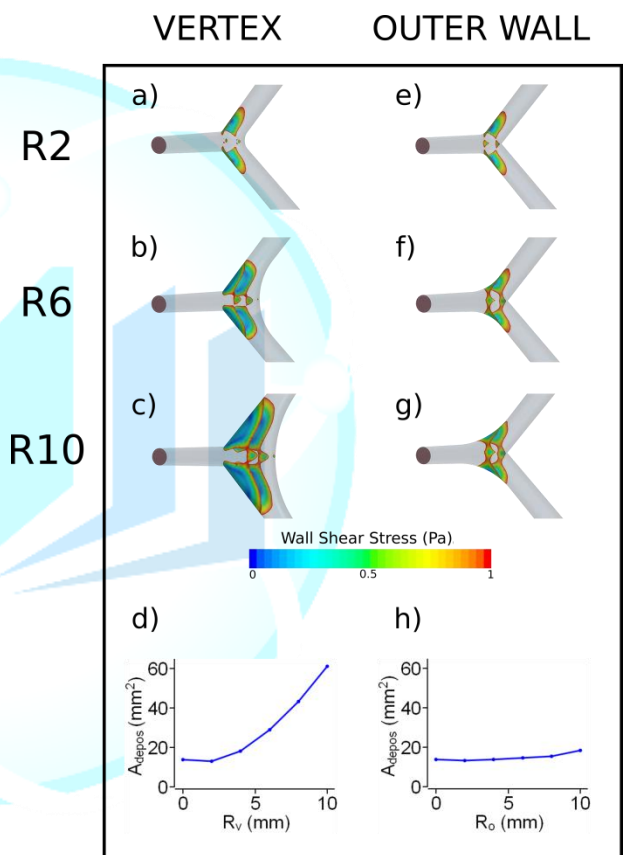


**Figure 4:** Effect of the radii of curvature ( $R_o$  and  $R_v$ ) at the symmetric bifurcation on the WSS distributions. (a)  $R_v=2 \text{ mm}$  and  $R_o=0 \text{ mm}$ . (b)  $R_v=6 \text{ mm}$  and  $R_o=0 \text{ mm}$ . (c)  $R_v=10 \text{ mm}$  and  $R_o=0 \text{ mm}$ . (d) Area with low WSS (less than  $1 \text{ Pa}$ ) or area of potential deposit versus  $R_v$  ( $R_o = 0 \text{ mm}$ ). (e)  $R_v=0 \text{ mm}$  and  $R_o=2 \text{ mm}$ . (f)  $R_v=0 \text{ mm}$  and  $R_o=6 \text{ mm}$ . (g)  $R_v=0 \text{ mm}$  and  $R_o=10 \text{ mm}$ . (h) Area with low WSS or area of potential deposit versus  $R_o$  ( $R_v = 0 \text{ mm}$ ).

Additionally, a constant pressure of  $10000 \text{ Pa}$  is considered in the outlets in order to simulate real conditions of artery pressure in coronary artery tree [33]. The size of the areas with WSS less than  $1 \text{ Pa}$  is studied. The analysis is performed in the systolic phase because it is in this part of the pulse when largest recirculation zones occur and five pulses are considered in order to stabilize the flow (Figure 6)

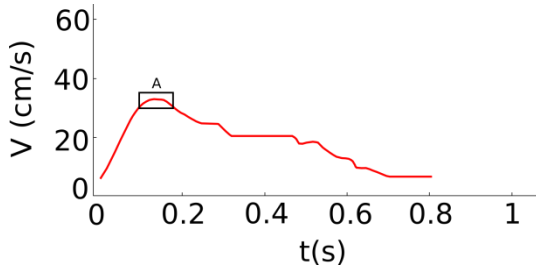


Figure 5: Cardiac pulse of 0.81 seconds length.

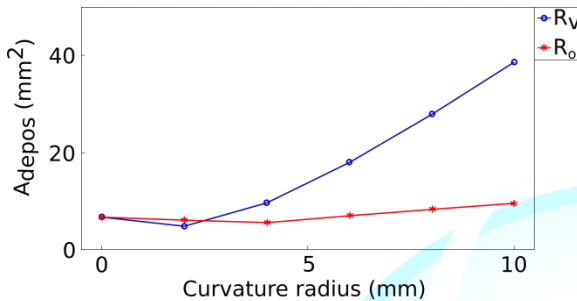


Figure 6: Area with low WSS (less than 1Pa) versus curvature radius on outer wall and on vertex considering a pulsatile flow.

Note that the results obtained are very similar to those presented in Figure 4. Thus, we can conclude that the vertex Radius of Curvature ( $R_v$ ) plays a significantly more important role than  $R_o$ . The velocity of the flow in the human vessels also varies depending on the proximity to the cardiac muscle or due to some other circumstances. Reynolds Number ( $Re$ ) is the ratio between inertial forces and viscous forces within a fluid and it is determined by the following equation [34]

$$Re = \frac{\rho D v}{\mu} \quad (4)$$

where  $v$  is the characteristic flow velocity,  $\rho$  the density,  $\mu$  the dynamic viscosity and  $D$  is the blood vessel diameter. This parameter is customarily used to describe the importance of the flow in vessels. In the following simulations, we consider the effect of  $Re$  on the possible deposition of plaque in the simulated vessels. The area of the regions characterized by low WSS (lower than 1 Pa) is the parameter to analyze (as in Figure 4) and we consider the variations introduced by the two radii of curvature at the vertex as well as the Reynolds number. Six different  $Re$  are considered ( $Re=106, 159, 212, 265, 318, 371$ ). These Reynolds numbers correspond with the following flow velocities ( $v=0.2, 0.3, 0.4, 0.5, 0.6$  and  $0.7$  m/s) that are reasonable values to be observed experimentally.

Figure 7 shows the effect of the two curvatures at the bifurcation ( $R_v$ , Figure 5a, and  $R_o$ , Figure 5b) on the deposition area or area with WSS smaller than 1 Pa for the different Reynolds numbers considered. Note that as the Reynolds number is increased, the areas where deposition could happen ( $A_{depos}$  characterized by  $WSS < 1$  Pa) decrease independently of the value of  $R_v$  or  $R_o$ . The additional kinetic energy of the fluid is used to improve the transport along the vessels. It is also observed that the influence of the curvature in the inner part of the bifurcation ( $R_v$  in Figure 7a) is stronger than  $R_o$  (Figure 7b) in good agreement with the results in figure 4. As the Reynolds number is decreased, the effect of  $R_v$  becomes more important and the areas with low WSS become more extended.

Figure 8 shows a comparison of the effect of the two curvature radii considering three different Reynolds numbers.  $A_{depos}$  (i.e. areas with low WSS) decreases as the Reynolds number increases in all configurations. Furthermore, as we increase the curvature radii, it is more evident that  $R_v$  has the predominant influence on the flow rather than  $R_o$ . A larger radius of curvature at the inner part of the bifurcation

results in larger areas of low WSS. This effect is also modulated by the Reynolds number. When the Reynolds number is equal to 106, areas with WSS less than 1 Pa begin to become significantly larger starting from  $R=4$ mm. When  $Re=265$  this happens from  $R=6$ mm and when  $Re=371$  it occurs from  $R=8$ mm. Thus, we observe that the influence of the geometry on WSS distribution is affected by the Reynolds number and therefore by the flow velocity. Note that the Reynolds number can also be affected by changing the physical properties of the fluid such as density or viscosity, via medication.

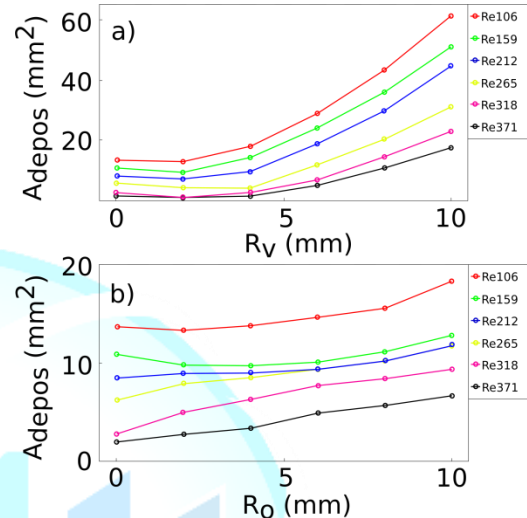


Figure 7: Area of deposition ( $A_{depos}$ ) versus (a) inner vertex curvature radius  $R_v$  (with  $R_o = 0$  mm) and (b) outer wall curvature radius  $R_o$  (with  $R_v = 0$  mm) for different values of the Reynolds number ( $Re$ ). The rest of the model parameters are kept as in the previous simulations.

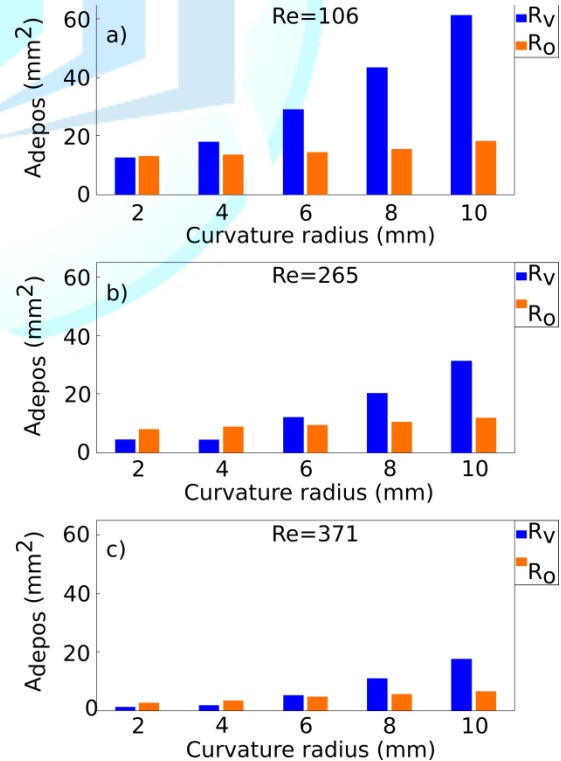
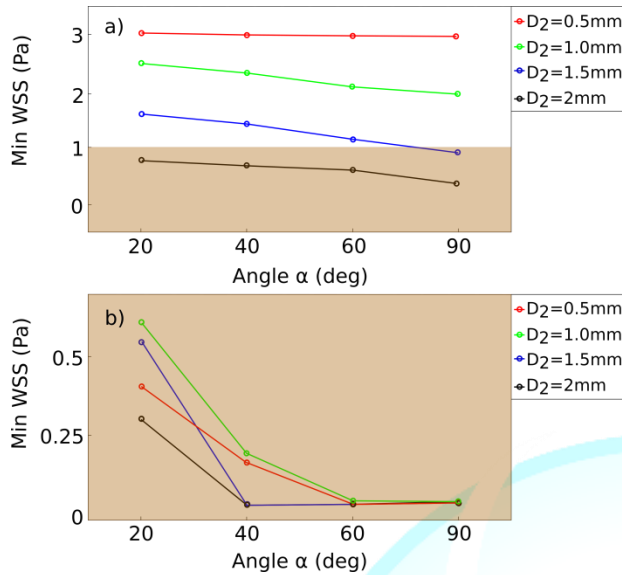


Figure 8: Variation of the deposition area ( $A_{depos}$ ) with the two curvature radii at the bifurcation ( $R_v$  and  $R_o$ ) for three different values of the Reynolds number; (a)  $Re=106$ , (b)  $Re=265$  and (c)  $Re=371$ .



### Non-symmetric geometry with $D_1=D_3$



**Figure 9:** Variation of the minimum values of WSS in (a) distal main vessel and (b) side vessel considering different angles (a) and side branch diameters ( $D_2$ ). Geometries with minimum WSS values are within the region colored in brown color are more prone to plaque formation.

In most of the coronary bifurcations the symmetric approximation considered in the previous section is not maintained. A non-symmetrical configuration is often seen, and the effect is the topic to analyze in the following. A vessel bifurcation as described in Figure 2 is considered with the diameter of the proximal main vessel ( $D_1$ ) equal to the distal main vessel diameter ( $D_3$ ). Thus, the two parameters to analyze are the diameter of the side branch ( $D_2$ ) and the angle of this vessel with the direction of the main vessel (a). Several simulations are done changing the values of the side vessel diameter ( $D_2=0.5, 1.0, 1.5$  and  $2$  mm) and the angle ( $\alpha = 20^\circ, 40^\circ, 60^\circ$  and  $90^\circ$ ). Note that in the main vessel, low WSS values occur right after the bifurcation at the outer wall while in the side branch, low WSS occurs in the outer wall immediately after the vertex bifurcation (see Figure 2 for locations).

The results are summarized in Figure 9. Figure 9a presents the minimum WSS plotted for each pair of  $D_2$  and  $\alpha$  for the main vessel after the bifurcation as recorded at the outer wall. This segment distal to the bifurcation point is one of the areas prone to plaque formation as can be observed in Figure 2. Note that, in general, as the angle or  $D_2$  become larger, the minimum WSS decreases. This effect is more dramatic for the case with  $D_2=1.5$  mm or larger, here increasing the angle produces values of the minimum of WSS below the values considered safe for plaque formation. The minimum WSS measured at the side branch are plotted in Figure 9b for the same cases considered in Figure 9a. The minimum WSS reaches a maximum for  $\alpha = 20^\circ$  independently on  $D_2$  and then drops, reaching a minimum value between  $\alpha = 60^\circ$  and  $\alpha=90^\circ$ . Note that all the values are below the threshold value (1 Pa) so the outer wall of the side branch in all cases simulated fulfills the conditions to accumulate plaque.

### Non-symmetric geometry following Finet's Law

This configuration becomes a step closer to a realistic situation where the distal main vessel reduces its diameter comparing with the proximal main vessel diameter as it happens in realistic configurations. Here, the diameter of the vessels is not conserved but it rather follows the Finet's law (Equation 3). The control parameters considered in these simulations are the inner diameter of the side branch ( $D_2$ ) that also defines the diameter of the distal main vessel ( $D_3$ ), and the angle at

the bifurcation ( $\alpha$ ). The results are summarized in Figure 10. Figure 10a shows the variation of the minimum WSS on the outer wall of the distal main vessel and Figure 10b the corresponding values of the side branch. Note that the value of  $D_2=0.5$  mm is not plotted as corresponds with a non-realistic configuration with a value of  $D_3$  larger than  $D_1$ . The behavior of the WSS in this second configuration is very similar to that observed in the first one (where proximal vessel radius and distal vessel radius were equal to 2mm in Figure 9). Geometries with a larger side branch radius present more risk to plaque formation in the mother vessel (Figure 10a). This effect is more significant when analyzing the side branch (Figure 10b). Note that now we also observe a minimum in the minimum WSS that is reached at  $\alpha = [60^\circ, 90^\circ]$  for all configurations. Nevertheless, the absolute values are significantly larger than in the previous case in Figure 9 mostly due to the reduction in the main distal vessel diameter ( $D_2$ ).

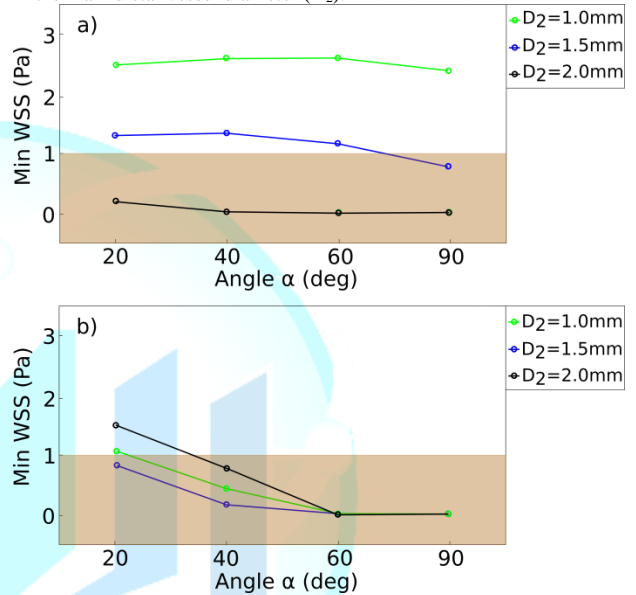


**Figure 10:** Variation of the minimum values of WSS in (a) the distal main (mother) vessel and (b) side vessel considering different angles and side branch diameters. Geometries whose minimum WSS values are within the region colored in brown color are more prone to plaque formation.

### Non-symmetric geometry Effect of the vertex topology

As with symmetrical bifurcations, it is important to know the influence of vertex shape of the non-symmetric bifurcations on the flow distribution and the location of those areas with low WSS. Thus, a study similar to those shown in Figure 4 is performed considering a bifurcation with an opening angle of  $60^\circ$  and the same diameter for all segments of the vessel (Figure 11). In Figure 11d and Figure 11h can be observed how the influence of the radius on the vertex on the size of the areas prone to plaque formation is much larger that the influence of the outer radius. Results are in good agreement with those obtained in section 3.1.

### Discussion

Bifurcations are ubiquitous in the arterial circulatory system as they play a crucial role in hemodynamics. Understanding their role on the fluid circulation is of crucial interest as they also play a negative role in the circulation as they might help in the deposition of spurious substances and conform the plaque and, eventually, help in developing diseases such as atherosclerosis. The specific geometry of the bifurcations has been demonstrated to strongly influence the formation of plaque. Along this manuscript we present results of numerical

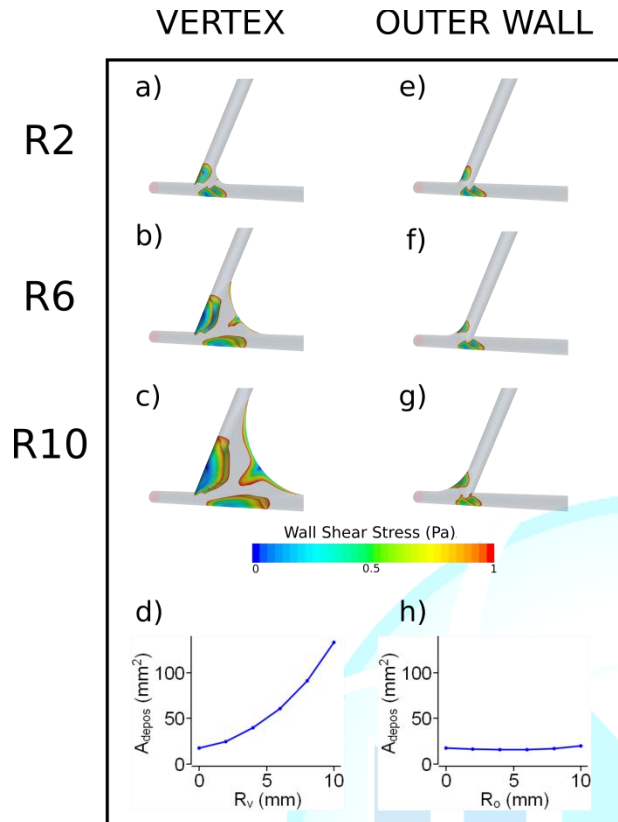


**Figure 11:** Effect of the radii of curvature ( $R_v$  and  $R_o$ ) at the non-symmetric bifurcation ( $\alpha=60^\circ$ ) on the WSS distributions. (a)  $R_v=2$  mm and  $R_o=0$  mm. (b)  $R_v=6$  mm and  $R_o=0$  mm. (c)  $R_v=10$  mm and  $R_o=0$  mm. (d) Area with low WSS (less than 1 Pa) or area of potential deposit versus  $R_v$  ( $R_o = 0$  mm). (e)  $R_v=0$  mm and  $R_o=2$  mm. (f)  $R_v=0$  mm and  $R_o=6$  mm. (g)  $R_v=0$  mm and  $R_o=10$  mm. (h) Area with low WSS or area of potential deposit versus  $R_o$  ( $R_v = 0$  mm).

simulations analyzing in detail different geometries of idealized vessels bifurcations. Two main aspects are the focus of this manuscript. First part is devoted to the effect of the topology of the vertex at the bifurcation on the flow circulation. Secondly, the analysis of the more-realistic non-symmetric bifurcations and the different parameters describing them.

The first part of the research identifies the important role played by the topology of the vertex itself. Any bifurcation is characterized by the curvature of the walls between the two daughter vessels after the branching (vertex radius of curvature,  $R_v$ ) and the curvature between the mother vessel and any of the daughter vessels (outer radius of curvature,  $R_o$ ). Our simulations clearly identify  $R_v$  as a critical parameter that can significantly increase the area of plaque deposition and, thus, the risk of coronary diseases. These results are in good agreement with those published by Perktold, et al., (1990) [35]. In this paper, authors analyzed T-shaped bifurcations (that could be considered as one of our limiting cases) and obtain that, in addition to the bifurcation angle, the sharpness/smoothness of the artery vertex significantly influence the local shear stress. In general, sharpened vertex lead to lower WSS. The effect of the flow characteristics, mainly determined by the Reynolds number, is also analyzed observing that large values of  $Re$  reduce the plaque deposition areas and, thus, coronary risks. This effect is found to be of major importance as it is one of the experimental parameters that physicians have to control hemodynamics.

The vessel flow is more unlikely to be modified without altering the normal heart functioning, but several drugs are commonly used to modify the effective viscosity (or even the density) of the circulating blood. Thus, understanding their influence on the coronary risk becomes crucial. In general, we observe that larger values of the Reynolds number reduce coronary risks at the bifurcations, and this can be achieved by significantly reducing the fluid viscosity without altering the heart rate. Considering different geometries of the bifurcations and different diameters for all the vessels involved, we are able to determine the critical parameters that produce the larger areas prone to produce plaque deposition.

This analysis was done for symmetric and non-symmetric bifurcations and our model allows to access to conditions and details that no experiment may reach. It is important to note that the use of mathematical models is becoming more popular as it allows to investigate a complete set of conditions with a detail in the resolution and the number of observables that it is not accessible via traditional in vivo experiments. This makes this type of research of great value for the scientific community as it provides with valuable information that it is not accessible otherwise and it is susceptible to be used in designing in-vivo experiments.

## Conclusion

The geometry of the coronary artery bifurcations plays a key role in the behavior of blood flow and in the location and size of areas prone to plaque formation. Thus, the vertex shape appears as the factor with a great influence in the distribution of areas with low WSS.

## Acknowledgments

We gratefully acknowledge financial support by the Spanish Ministerio de Economía y Competitividad and European Regional Development Fund under contract RTI2018-097063-BI00 AEI/FEDER, UE, and by Xunta de Galicia under Research Grant No. 2021-PG036-1. Authors are part of the CITMaga Strategic Partnership (AGRUP2015/02). All these programs are cofunded by FEDER (UE).

## References

1. Ku DN, Giddens DP, Zarins CK and Glagov S. Pulsatile flow and atherosclerosis in the human carotid bifurcation. Positive correlation between plaque location and low oscillating shear stress (1985) *Arteriosclerosis: An Official J American Heart Association Inc* 5: 293-302. <https://doi.org/10.1161/01.ATV.5.3.293>
2. Langille BI and O'Donnell F. Reductions in arterial diameter produced by chronic decreases in blood flow are endothelium dependent (1986) *Sci* 231: 405-407. <https://doi.org/10.1126/science.3941904>
3. LaBarbera, M. Principles of design of fluid transport systems in zoology (1990) *Sci* 249: 992-1000. <https://doi.org/10.1126/science.2396104>
4. Malek AM, Alper SL and Izumo S. Hemodynamic shear stress and its role in atherosclerosis (1999) *Jama* 282: 2035-2042. <https://doi.org/10.1001/jama.282.21.2035>
5. Asakura T and Karino T. Flow patterns and spatial distribution of atherosclerotic lesions in human coronary arteries (1990) *Circulation research* 66: 1045-1066. <https://doi.org/10.1161/01.res.66.4.1045>
6. Tropea BI, Glagov S and Zarins CK. Hemodynamics and atherosclerosis (1997) *The Basic Science of Vascular Disease*.
7. Ungvári T, Sánta J, Béres Z, Tar B, Sánta P, et al., Evaluation of the spatial changes of the coronary morphology due to stent implantation with three-dimensional angiography (2009) In 2009 36th Annual Computers in Cardiology Conference (CinC) 649-651 IEEE.



8. Eom H.J, Yang DH, Kim YH, Roh JH, Kweon J, et al., Coronary bifurcation stent morphology in dual-source CT: validation with micro-CT (2016) *Int J cardiovas imaging* 32: 1659-1665. <https://doi.org/10.1007/s10554-016-0953-6>
9. Okano M. and Yoshida Y. Junction complexes of endothelial cells in atherosclerosis-prone and atherosclerosis-resistant regions on flow dividers of brachiocephalic bifurcations in the rabbit aorta (1994) *Biorheology* 31: 155-161. <https://doi.org/10.3233/bir-1994-31203>
10. Shaaban AM and Duerinckx AJ. Wall shear stress and early atherosclerosis: a review (2000) *Americ J Roentgenology* 174: 1657-1665. <https://doi.org/10.2214/ajr.174.6.1741657>
11. Otero-Cacho A, Aymerich M, Flores-Arias MT, Abal M, Álvarez E, et al., Determination of hemodynamic risk for vascular disease in planar artery bifurcations (2018) *Scientific reports* 8: 1-7. <https://doi.org/10.1038/s41598-018-21126-1>
12. Bonert M, Leask RL, Butany J, Ethier CR, Myers JG. The relationship between wall shear stress distributions and intimal thickening in the human abdominal aorta (2003) *Biomedical engineering online* 2: 18. <https://doi.org/10.1186/1475-925x-2-18>
13. Bajraktari A, Bytyçi I and Henein MY. The Relationship between Coronary Artery Wall Shear Strain and Plaque Morphology: A Systematic Review and Meta-Analysis (2020) *Diagnostics* 10: 91. <https://doi.org/10.3390/diagnostics10020091>
14. Mongrain R. and Rodés-Cabau J. Role of shear stress in atherosclerosis and restenosis after coronary stent implantation (2006) *Revista española de cardiología* 59: 1-4. [https://doi.org/10.1016/S1885-5857\(06\)60040-6](https://doi.org/10.1016/S1885-5857(06)60040-6)
15. Morbiducci U, Kok AM, Kwak BR, Stone PH, Steinman DA, et al., Atherosclerosis at arterial bifurcations: evidence for the role of hemodynamics and geometry (2016) *Thromb Haemost* 115: 484-492. <https://doi.org/10.1160/th15-07-0597>
16. Pinho N, Sousa LC, Castro CF, António CC, Carvalho M, et al., The Impact of the Right Coronary Artery Geometric Parameters on Hemodynamic Performance (2019) *Cardiovas eng tech* 10: 257-270. <https://doi.org/10.1007/s13239-019-00403-8>
17. Gallo D, Steinman DA, Bijari PB and Morbiducci U. Helical flow in carotid bifurcation as surrogate marker of exposure to disturbed shear (2012) *J biomech* 45: 2398-2404. <https://doi.org/10.1016/j.jbiomech.2012.07.007>
18. Frattolin J, Zarandi MM, Pagiatakis C, Bertrand OF and Mongrain R. Numerical study of stenotic side branch hemodynamics in true bifurcation lesions (2015) *Comp Bio Med* 57: 130-138. <https://doi.org/10.1016/j.compbiomed.2014.11.014>
19. Chiastra C, Gallo D, Tasso P, Iannaccone F, Migliavacca F, et al., Healthy and diseased coronary bifurcation geometries influence nearwall and intravascular flow: a computational exploration of the hemodynamic risk (2017) *J biomech* 58: 79-88. <https://doi.org/10.1016/j.jbiomech.2017.04.016>
20. Beier S, Ormiston J, Webster M., Cater J, Norris S, et al., Impact of bifurcation angle and other anatomical characteristics on blood flow—A computational study of non-stented and stented coronary arteries (2016) *J biomech* 49: 1570-1582. <https://doi.org/10.1016/j.jbiomech.2016.03.038>
21. Malvè M, García A, Ohayon J and Martínez MA. Unsteady blood flow and mass transfer of a human left coronary artery bifurcation: FSI vs. CFD (2012) *Int communications in heat and mass transfer* 39: 745-751. <https://doi.org/10.1016/j.icheatmasstransfer.2012.04.009>
22. Finet G, Gilard M, Perrenot B, Rioufol G, Motreff P, et al., Fractal geometry of arterial coronary bifurcations: a quantitative coronary angiography and intravascular ultrasound analysis. *EuroIntervention* (2018) journal of EuroPCR in collaboration with the Working Group on Interventional Cardiology of the European Society of Cardiology 3: 490- 498. <https://doi.org/10.4244/eijv3i4a87>
23. Rigatelli G, Zuin M, Ronco F, Caprioglio F, Cavazzini D, et al., Usefulness of the Finet law to guide stent size selection in ostial left main stenting: Comparison with standard angiographic estimation (2018) *Cardio Revas Med* 19: 751-754. <https://doi.org/10.1016/j.carrev.2018.04.005>
24. Gwon HC. Understanding the coronary bifurcation stenting (2018) *Korean Circulation J* 48: 481-491. <https://doi.org/10.4070/kcj.2018.0088>
25. Hoye A. The proximal optimisation technique for intervention of coronary bifurcations (2017) *Int Cardio Review* 12: 110. <https://doi.org/10.15420/icr.2017.11:2>
26. <https://thesteveportal.plm.automation.siemens.com>
27. Ferziger JH, Peric M and Robert L. Street (2018) *Computational Methods for Fluid Dynamics*, Cham: Springer, 16: 37.
28. Patankar SV and Spalding DB. A calculation procedure for heat, mass and momentum transfer in three-dimensional parabolic flows (1983) *Numerical prediction of flow, heat transfer, turbulence and combustion*, 54-73. <https://doi.org/10.1016/b978-0-08-030937-8.50013-1>
29. Kim HJ, Vignon-Clementel IE, Figueroa CA, LaDisa JF, Jansen KE, et al., On coupling a lumped parameter heart model and a three-dimensional finite element aorta model (2009) *Annals of biomedical engineering* 37: 2153-2169. <https://doi.org/10.1007/s10439-009-9760-8>
30. Chodzyński KJ, Boudjeltia KZ, Lalmand J, Aminian A, Vanhamme L, et al., An in vitro test bench reproducing coronary blood flow signals (2015) *Biomed engineer online* 14: 77. <https://doi.org/10.1186/s12938-015-0065-x>
31. Decorato I, Kharboutly Z, Vassallo T, Penrose J, Legallais C, et al., Numerical simulation of the fluid structure interactions in a compliant patient-specific arteriovenous fistula (2014) *Int j numerical methods biomed eng* 30: 143-159. <https://doi.org/10.1002/cnm.2595>
32. Byun JS, Choi SY and Seo T. The numerical study of the hemodynamic characteristics in the patient-specific intracranial aneurysms before and after surgery (2016) *Computational and mathematical methods in medicine*, 2016. <https://doi.org/10.1155/2016/4384508>
33. Sinnott M, Cleary PW and Prakash M. An investigation of pulsatile blood flow in a bifurcation artery using a grid-free method (2016) *In Proc. Fifth International Conference on CFD in the Process Industries* 1-6.
34. Shashi E. *Transmission Pipeline Calculations and Simulations Manual* (2015).
35. Perktold K and Peter R Numerical 3D-simulation of pulsatile wall shear stress in an arterial T-bifurcation model (1990) *J biomed engin* 12: 2-12. [https://doi.org/10.1016/0141-5425\(90\)90107-x](https://doi.org/10.1016/0141-5425(90)90107-x)